



Mohjazi, L. , Muhaidat, S., Abbasi, Q. H. , Imran, M. A. , Dobre, O. A. and Di Renzo, M. (2021) Battery recharging time models for reconfigurable intelligent surfaces-assisted wireless power transfer systems. *IEEE Transactions on Green Communications and Networking*, 6(2):1173-1185, (doi: [10.1109/TGCN.2021.3120834](https://doi.org/10.1109/TGCN.2021.3120834))

The material cannot be used for any other purpose without further permission of the publisher and is for private use only.

There may be differences between this version and the published version. You are advised to consult the publisher's version if you wish to cite from it.

<http://eprints.gla.ac.uk/256843/>

Deposited on 14 October 2021

Enlighten – Research publications by members of the University of
Glasgow

<http://eprints.gla.ac.uk>

Battery Recharging Time Models for Reconfigurable Intelligent Surfaces-Assisted Wireless Power Transfer Systems

Lina Mohjazi, *Senior Member, IEEE*, Sami Muhaidat, *Senior Member, IEEE*, Qammer H. Abbasi, *Senior Member, IEEE*, Muhammad Ali Imran, *Senior Member, IEEE*, Octavia A. Dobre, *Fellow, IEEE*, and Marco Di Renzo, *Fellow, IEEE*

Abstract—In this paper, we develop an analytical framework for the statistical analysis of the battery recharging time (BRT) in reconfigurable intelligent surfaces (RISs)-aided wireless power transfer (WPT) systems. Specifically, we derive novel closed-form expressions for the probability density function (PDF), cumulative distribution function, and moments of the BRT of the radio frequency energy harvesting wireless nodes. Moreover, a closed-form expression of the PDF of the BRT is obtained for the special case when the RIS consists of a large number of elements. Capitalizing on the derived expressions, we offer a comprehensive treatment for the statistical characterization of the BRT and study the impact of the system and battery parameters on its performance. Our results reveal that the proposed statistical models are analytically tractable, accurate, and efficient in assessing the sustainability of RIS-assisted WPT networks and in providing key design insights for large-scale future wireless applications. For example, we demonstrate that a 4-fold reduction in the mean time of the BRT can be achieved by doubling the number of RIS elements. Monte Carlo simulation results corroborate the accuracy of the proposed theoretical framework.

Index Terms—Reconfigurable intelligent surfaces (RIS), statistical models, wireless power transfer, recharging time.

I. INTRODUCTION

THE roadmap to beyond fifth generation (B5G) wireless networks is envisaged to introduce a new spectrum of fully automated and intelligent data-driven services, such as flying vehicles, haptics, telemedicine, augmented and virtual reality [1]–[5]. Several unprecedented application environments, including machine-to-people and machine-to-machine communications, are expected to be the driving force of B5G systems. As a result, the number of connected Internet-of-Everything (IoE) devices (e.g., sensors, wearables, implant-

ables, tablets) is anticipated to witness a phenomenal growth in the next few years, reaching up to tens of billions [6]. This poses a fundamental challenge on provisioning a ubiquitous seamless connectivity, while concurrently prolonging the lifetime of a massive number of energy-constrained low-power low-cost devices.

Wireless power transfer (WPT) has been highly recognized in both academia and industry as a promising technology to address the energy sustainability problem of wireless nodes, and has rapidly gained growing interest in the context of B5G communication networks [7], [8]. This is mainly due to its capability to deliver on-demand wireless energy to a large number of wireless devices in a controllable and low-cost manner, and thus, eliminating the need for battery replacement. In this framework, radio frequency (RF) signals, that are received from dedicated wireless power transmitters, are leveraged either to recharge the batteries of wireless nodes or to directly power the wireless transmissions of battery-less devices [9], [10].

However, it is demonstrated in recent studies [11]–[13] that, the distance between the RF transmitter and the corresponding RF energy harvesting (RFEH) receiver creates a performance bottleneck for practical wirelessly-powered wireless networks. This stems from the fact that the efficiency of WPT is inversely proportional to the distance, and hence, conventional relay-aided wireless communications were proposed to realize WPT range expansion [11]–[13]. More recently, advanced technologies, such as massive multiple-input multiple-output (MIMO), have been studied as potential candidates to achieve considerable WPT efficiency gains through the exploitation of beamforming with or without relaying techniques [14], [15]. Nonetheless, this comes at the price of severe energy consumption, higher computational complexity, and increased hardware cost, all of which are more pronounced at higher RF frequencies, such as millimeter-wave frequencies for future wireless systems [16]. In addition to the distance factor, the efficiency of WPT, achieved through these conventional mechanisms, is degraded by the RF signal attenuation resulting from high penetration loss, multi-path fading, molecular absorption, and Doppler shift [3]. This effect is even more noticeable in ultra-dense network deployments, which feature highly dynamic radio environments.

To address the aforementioned challenges, *reconfigurable intelligent surfaces* (RISs) have recently emerged as a prom-

L. Mohjazi, Q. H. Abbasi, and M. A. Imran are with the James Watt School of Engineering, University of Glasgow, Glasgow, G12 8QQ, UK (e-mail: l.mohjazi@ieee.org, {Qammer.Abbasi, Muhammad.Imran}@glasgow.ac.uk).

S. Muhaidat is with the Center for Cyber-Physical Systems, Department of Electrical Engineering and Computer Science, Khalifa University, Abu Dhabi 127788, UAE, and also with the Department of Systems and Computer Engineering, Carleton University, Ottawa, ON K1S 5B6, Canada (e-mail: muhaidat@ieee.org).

O. A. Dobre is with the Faculty of Engineering and Applied Science, Memorial University, A1B 3X5, Canada (e-mail: odobre@mun.ca).

M. Di Renzo is with Université Paris-Saclay, CNRS, CentraleSupélec, Laboratoire des Signaux et Systèmes, 3 Rue Joliot-Curie, 91192 Gif-sur-Yvette, France (marco.di-renzo@universite-paris-saclay.fr). The work of M. Di Renzo was supported in part by the European Commission through the H2020 ARIADNE project under grant agreement number 871464 and through the H2020 RISE-6G project under grant agreement number 101017011.

ising technology that can potentially offer fundamental performance improvements in wireless systems, in terms of spectrum and energy efficiencies, in a cost-effective manner [1]–[3], [17]–[19]. Practically, RISs can be realized by different approaches. This includes (i) surfaces equipped with large arrays of discrete, inexpensive, and tiny antenna elements, called unit cells, (ii) implementations based on conformal large surfaces or metamaterial-based planar surfaces with scattering elements spaced apart at distances much smaller than the wavelength [20]. Unlike conventional approaches that lack full control over the propagation environment, RISs allow a transformative control of the electromagnetic (EM) waves [1], [4], [20]. For example, in RISs made of large arrays of inexpensive antennas, each element is individually configured and optimized to manipulate the impinging EM waves in arbitrary ways [21], [22]. This is achieved by jointly manipulating the reflected signal amplitude and/or phase shift at each of the RIS elements in real time according to the dynamic and implicit randomness of wireless channels. For instance, the signal component arriving from an RF source node and reflected by the RIS elements can be steered towards an intended destination node to enhance its received signal power. Traditional transmission techniques, such as phased arrays, multi-antenna transmitters, and relays, involve active components of complex hardware that exhibit high power consumption. On the other hand, RISs require a large number of scattering elements that are coupled with a number of small-sized, low-power, and inexpensive components [21], [22]. Details of the key similarities and differences between RIS and relays are provided in [23].

As a consequence of the aforementioned advantages offered by RISs compared to conventional relaying techniques, the application of RISs is recognized to be particularly appealing for aiding in WPT systems [4]. This is due to the fact that the large aperture of RISs is leveraged to assist in powering a massive number of heterogeneous devices by compensating the significant power loss over long distances via appropriately customized signal reflections. This yields a substantial improvement of the overall efficiency of WPT systems.

A. Related Work

The opportunities opened by RISs have spurred, in a short span of time, research in many areas related to wireless communication systems. This includes multi-user resource allocation, beamforming optimization, design of efficient enabling mechanisms, and performance analysis of RIS-assisted wireless networks. For example, in the area of resource allocation, the authors of [24] developed energy-efficient power allocation approaches subject to individual link budget guarantees for multiple mobile users. The authors of [25] proposed an achievable rate optimization framework for orthogonal frequency division multiplexing (OFDM) that jointly identifies the transmit power at the base station (BS) and the reflection coefficients at the RIS. Furthermore, several research works designed enabling mechanisms, such as channel estimation schemes, in an effort to achieve the passive beamforming gains of RISs [26], [27]. Also, to reduce the overhead in channel training, the authors of [28] proposed a practical

transmission protocol that involves estimating the combined channel of a group of RIS elements. Furthermore, the authors of [29] and [30] investigated the realization of index modulation and space-time modulated digital coding, respectively, in RIS-assisted transmissions to improve the spectral efficiency. From the performance analysis point of view, recent research studies provided a theoretical framework to characterize the performance of RIS-assisted wireless systems in terms of outage probability [31], reflection probability [32], spectral efficiency [33], [34], and capacity [35]–[37]. Additionally, the fundamental limits of the error probability performance of RIS-aided backscatter and non-orthogonal multiple access (NOMA) were examined in [38] and [39], respectively. Furthermore, numerous research studies focused on proposing active and passive beamforming strategies to achieve secrecy [40] and sum-rate [41] enhancements and transmit power reduction [42]–[44] for multi-antenna and/or multi-user RIS-assisted networks.

While the preceding research works focus on leveraging the benefits of RISs to improve the performance of information transfer, RISs are shown to offer significant enhancements in terms of power transfer efficiency in wireless systems powered by near-field WPT [45]. Apart from this, the deployment of RISs is demonstrated to enhance the far-field WPT and establish effective RFEH zones through compensating the attenuation of RF signals over long distances [46]–[48]. Specifically, the authors of [46] and [47] considered the weighted sum-power and sum-rate optimization problems, respectively, for RIS-aided simultaneous wireless information and power transfer (SWIPT) systems, where an RIS is deployed in the vicinity of two separate groups of energy and information receivers. Moreover, joint active and passive beamforming design for RIS-aided SWIPT systems is proposed in [48], by taking into consideration the signal-to-interference-plus-noise ratio constraints imposed by the information receivers (IRs) and the RFEH constraints imposed by the energy receivers (ERs).

B. Motivation and Contribution

The aforementioned studies [46]–[48] assume battery-free RFEH ERs, whose harvested energy is directly used for future transmissions. In this case, the received RF signals, and consequently, the amount of harvested energy, is considered to be sufficient and predictable over a certain period of time. In scenarios where RFEH nodes are equipped with batteries [49], however, the harvested energy is first stored in the battery before being used for future transmissions. Since the power of the received RF signal depends on the distribution of the wireless fading channel between the transmitter and the receiver, the RFEH process and, similarly, the time required to recharge the battery of an RFEH node, called the battery recharging time (BRT), are stochastic processes. The statistical characterization and modeling of the BRT were developed in [49]–[51] for conventional SWIPT systems operating over multi-path fading channels. Their results demonstrated that the RFEH process is significantly impacted by the system, fading, and battery parameters, including the capacity and discharging depth, and the BRT. Although the previously

mentioned research works [46]–[48] provide useful results to improve the RFEH process in RIS-assisted SWIPT systems, their approach focuses on developing transmission protocols and their design insights are limited to battery-free ERs.

Despite being a fundamental figure of merit in designing and quantifying the sustainability of RIS-assisted WPT networks in various operational setups in B5G systems, to the best of our knowledge, the statistical characterization of the BRT is not yet studied in the open literature. Motivated by this, the prime focus of this work is to develop a novel theoretical framework to characterize the statistical properties of the BRT for RIS-assisted WPT systems, consisting of ERs with limited battery capacity. In our work, we consider that the RIS comprises passive reflecting elements spaced half of the wavelength apart, and that each element is individually configured for realizing optimal WPT. The main contributions of this paper are listed as follows:

- First, we derive novel accurate closed-form approximations for the probability density function (PDF) and cumulative distribution function (CDF) of the instantaneous total received power of the energy harvesting node. The obtained expressions take into account the number of RIS elements and the distances of the source (S)→RIS and RIS→ER links, and assume that all wireless channels are subject to Rayleigh fading.
- Building upon the analytical expressions of the received power, we obtain closed-form expressions for the PDF and CDF of the BRT. The derived results are shown to accurately capture the impact of the battery parameters (i.e., discharge depth, battery capacity, and charging voltage), system parameters, and the number of RIS elements on the BRT statistical properties. To the best of our knowledge, these expressions are novel in literature.
- Next, an analytical closed-form expression for the PDF of the BRT is derived for the special case when the number of RIS elements grows large. In this case, we exploit the central limit theorem (CLT) to demonstrate that the PDF of the BRT converges to an impulse response, revealing that the deployment of RISs is highly promising in practically realizing WPT in future large-scale IoE networks.
- To further investigate the properties of the BRT, we derive a computationally simple closed-form expression for its moments. We employ this result to obtain statistical tools to evaluate the mean value, variance, skewness and kurtosis of the BRT.
- The derived expression of the moments is also exploited to examine the amount of fading (AoF) of the BRT as a function of the RIS elements. Our study unveils that, employing RISs of large size can effectively boost the efficiency of WPT over fading channels.
- Finally, we present Monte Carlo simulation and numerical results to validate the accuracy of the developed theoretical framework.

C. Organization

The rest of the paper is organized as follows: Section II introduces the RIS-assisted WPT system model, as well as the

statistical characterization of the corresponding power received by the energy harvesting node. In Section III, the analytical expressions of the statistics of the BRT for RIS-assisted WPT systems are derived. Simulation and numerical results are presented in Section IV, while concluding remarks are given in Section V.

II. SYSTEM AND CHANNEL MODEL

In this paper, we consider a single-antenna RF source node, S , and a single-antenna energy-constrained ER, as depicted in Fig. 1. The ER could be a low-power sensor node equipped with a battery with a finite capacity. In order to extend the operational range of the ER, while ensuring that its harvested energy is sufficient for real-life operation, we propose a WPT system assisted by an RIS.

The end-to-end (E2E) channel gain between S and the ER characterizes the power received at the ER, and accordingly, defines the behavior of the overall RFEH process, including the instantaneous BRT at the ER. Therefore, to quantify the impact of RIS-assisted WPT on the required time to charge the battery of the ER node, we analytically present the distribution of the instantaneous received power at the ER, which will be exploited next to develop the statistical characterization of the underlying instantaneous BRT.

We further assume that the direct link does not exist between S and the ER. This is motivated by the fact that this link is subject to strong attenuation, due to deep fading or shadowing effects due to surrounding physical obstacles, and WPT can be achieved only via the RIS. It is worth mentioning that such an assumption is widely adopted in research studies related to WPT systems [12], [47]. Moreover, this assumption is usually employed in the literature of RIS-assisted communications [52], [53], since an RIS is more useful in environments that experience a high blockage probability [54], [55].

In our setup, we consider an RIS that is made of N elements. Each of the elements can be reconfigured through software by using a controller, as illustrated in Fig. 1. The power transmitted from S , being either a BS or an RF source, which is reflected by the RIS towards the ER, is harvested and stored in a battery with a limited capacity before being used in future signal transmissions.

As shown in the block diagram of Fig. 1, h_i and g_i denote the small scale complex channel fading coefficients of the $S \rightarrow \text{RIS}$ and $\text{RIS} \rightarrow \text{ER}$ links, respectively, where $i \in \{1, 2, \dots, N\}$ denotes the i -th element of RIS. The envelopes of the two wireless links are modeled as independent and identically distributed (i.i.d) Rayleigh fading channels with the scale parameter, σ , being equal to 1, i.e., $|h_i|, |g_i| \sim \mathcal{CN}(0, 2\sigma^2)$ for $i \in \{1, 2, \dots, N\}$, where $\mathcal{CN}(0, \kappa)$ stands for a zero-mean complex Gaussian distribution with variance equal to κ . The assumption of Rayleigh fading channels is representative of scenarios in which a line-of-sight (LoS) link cannot be established. Although channels in RIS-assisted wireless communications are often characterized by a LoS connection, there are scenarios where the LoS may not be available, e.g., when the RISs are deployed on randomly distributed spatial blockages, and a significant number of

scatterers still exist. In this case, the system designer has no control on the optimal location of RISs [56]. Therefore, in this work, we consider that the LoS is unavailable, and hence, wireless communication is carried out over the non-LoS (NLoS) component only. It is worth mentioning that this assumption is made in other related research works, such as [2], [52], [53], [57] and the references therein.

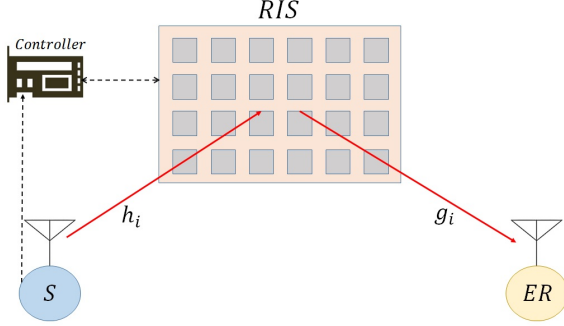


Figure 1: RIS-assisted WPT system model.

Let P_s denote the transmit wireless power of the source node. The instantaneous total power received at the ER through the i -th element of RIS is expressed as

$$P_r = \frac{\left| \sum_{i=1}^N |h_i| |g_i| e^{j\theta_i} \right|^2}{d_1^\delta d_2^\delta} P_s, \quad (1)$$

where d_1 and d_2 represent the distance between S and the center of the RIS and between the center of the RIS and the ER, respectively, and δ is the path loss exponent. Furthermore, θ_i specifies the adjustable phase induced by the i -th element of the RIS [2]. The total received power in (1) is based on the path loss model $1/\sqrt{d_1^\delta d_2^\delta}$ that is applicable in the far-field regime, as defined in [58], [59]. Accordingly, N can be large but it needs to be finite [20, Sec. IV-D].

It is assumed that the channel phases of h_i and g_i , denoted as ϕ_{h_i} and ϕ_{g_i} , respectively, are perfectly known to the RIS and, accordingly, it is able to apply optimal phase shifts, i.e., $\theta_i = -(\phi_{h_i} + \phi_{g_i})$ [60]. This assumption constitutes a system operation performance benchmark for practical operations [2]. Therefore, the obtained results represent a lower bound on the BRT required to sustain the operation of RIS-assisted WPT systems. In this paper, we assume that the amplitude of the reflection coefficient of each RIS element is equal to 1,¹ for all $i \in N$. Consequently, the instantaneous received power is maximized and (1) can be formulated as

$$P_r = \frac{P_s}{d_1^\delta d_2^\delta} B^2 \quad (2)$$

where

$$B = \sum_{i=1}^N |h_i| |g_i| \quad (3)$$

is the E2E channel gain.

¹Recent studies proposed efficient designs achieving a reflection coefficient value as high as one [4].

A. Statistical Characterization of the E2E Channel

As previously mentioned, the BRT, T_r , is determined by the amount of power received and then harvested at the ER. Therefore, it is necessary to have in hand the statistical characterization of the E2E channel fading coefficient, B , in order to derive the distributions of P_r and T_r . Note that B presents a sum of N double Rayleigh random variables (RVs). An accurate approximation of its PDF is given in the following proposition.

Proposition 1: *The PDF of the E2E channel coefficient of an RIS-assisted WPT system is accurately approximated in a closed-form expression as*

$$f_B(x) \approx a_1 G_{1,2}^{2,0} \left[\frac{x}{a_2} \middle| \begin{matrix} -; a_3 \\ a_4, a_5; - \end{matrix} \right], x \geq 0, \quad (4)$$

where $G_{\cdot,\cdot}^{a,b}[\cdot]$ denotes the Meijer G-function defined in [61, Eq. (8.2.1.1)] and

$$a_1 = \frac{\Gamma(a_3 + 1)}{a_2 \Gamma(a_4 + 1) \Gamma(a_5 + 1)}, \quad (5)$$

$$a_3 = \frac{4\varphi_4 - 9\varphi_3 + 6\varphi_2 - \mu_1}{-\varphi_4 + 3\varphi_3 - 3\varphi_2 + \mu_1}, \quad (6)$$

$$a_2 = \frac{a_3}{2} (\varphi_4 - 2\varphi_3 + \varphi_2) + 2\varphi_4 - 3\varphi_3 + \varphi_2, \quad (7)$$

$$a_4 = \frac{a_6 + a_7}{2}, \quad (8)$$

$$a_5 = \frac{a_6 - a_7}{2}, \quad (9)$$

with

$$a_6 = \frac{a_3 (\varphi_2 - \mu_1) + 2\varphi_2 - \mu_1}{a_2} - 3, \quad (10)$$

$$a_7 = \sqrt{\left(\frac{a_3 (\varphi_2 - \mu_1) + 2\varphi_2 - \mu_1}{a_2} - 1 \right)^2 - 4 \frac{\mu_1 (a_3 + 1)}{a_2}}, \quad (11)$$

and

$$\varphi_j = \frac{\mu_j}{\mu_{j-1}}, j > 1. \quad (12)$$

Also, μ_j is the j -th moment of B and $\Gamma(\cdot)$ is the Gamma function defined in [62, Eq. (6.1.1)].

Proof: The RV B , given in (3), is written as a sum of the RVs $|h_i| |g_i|$. Therefore, its PDF can be formulated in a closed-form in an approximated expression by using the moment-based density approximants method presented in [63]. The evaluation of the first four moments, ensuring an accurate approximation for the PDF of B , are obtained in [64] and are presented here for clarity and completeness of the work. Specifically, the first, second, third, and fourth moments are expressed as (13), (14), (15), and (16), respectively. This completes the proof.

$$\mu_1 = \frac{N\pi}{2}, \quad (13)$$

$$\mu_2 = \left(4 + (N-1) \frac{\pi^2}{4} \right) N, \quad (14)$$

$$\mu_4 = \begin{cases} \left(64N + 48N(N-1) + 9N(N-1)\pi^2 + 6N(N-1)(N-2)\pi^2 + \frac{N(N-1)(N-2)(N-3)\pi^4}{16} \right), N \geq 4 \\ (480 + 90\pi^2), N = 3 \\ (224 + 18\pi^2), N = 2 \\ 64, N = 1. \end{cases} \quad (16)$$

$$\mu_3 = \begin{cases} N\pi \left(\frac{9}{2} + 6(N-1) + (N-1)(N-2)\frac{\pi^2}{8} \right), N \geq 3 \\ 9\pi + 3 \times 2 \times \frac{\pi}{2} \times 4 = 21\pi, N = 2 \\ \frac{9\pi}{2}, N = 1. \end{cases} \quad (15)$$

Based on the PDF obtained in (4), an accurate approximation for the CDF of B can be analytically computed as [63]

$$F_B(x) \approx a_1 a_2 G_{2,3}^{2,1} \left[\frac{x}{a_2} \middle| \begin{matrix} 1; a_3 + 1 \\ a_4 + 1, a_5 + 1; 0 \end{matrix} \right], x \geq 0. \quad (17)$$

The result obtained in Proposition 1 and the expression given in (17) enable us to derive the statistical characterization of the received power at the ER, and hence, the statistical distributions of the BRT. It can be observed from Proposition 1 and (17) that the E2E channel gains depend on the number of RIS elements N . Accordingly, we expect that the received power as well as the BRT will depend on N , as will be demonstrated next.

B. Statistical Characterization of the Received Power

Capitalizing on the statistical model of the E2E channel gain presented in the previous section, we derive the distribution of the instantaneous total received power at the ER in the following proposition.

Proposition 2: *For an RIS-assisted WPT system, the CDF of the instantaneous power received at the ER node can be expressed as*

$$F_{P_r}(x) \approx a_1 a_2 G_{2,3}^{2,1} \left[\frac{1}{a_2} \sqrt{\frac{x}{\bar{P}_r}} \middle| \begin{matrix} 1; a_3 + 1 \\ a_4 + 1, a_5 + 1; 0 \end{matrix} \right], x \geq 0. \quad (18)$$

Proof: The CDF of P_r is given as

$$F_{P_r}(x) = \Pr(P_r \leq x). \quad (19)$$

Substituting (2) in (19) yields

$$F_{P_r}(x) = \Pr \left(B \leq \sqrt{\frac{x}{\bar{P}_r}} \right) \quad (20)$$

or equivalently

$$F_{P_r}(x) = F_B \left(\sqrt{\frac{x}{\bar{P}_r}} \right), \quad (21)$$

where

$$\bar{P}_r = \frac{P_r}{d_1^\delta d_2^\delta} \quad (22)$$

denotes the average power received at the ER. By invoking the expression given in (17), (18) can be obtained, which

concludes the proof. \blacksquare

Accordingly, the PDF of P_r can be obtained by applying [65, Eq. (07.34.20.0001.01)] to differentiate (18), i.e.,

$$f_{P_r}(x) = \frac{dF_{P_r}(x)}{dx}, \quad (23)$$

yielding

$$f_{P_r}(x) \approx \frac{a_1 a_2}{2x} G_{1,2}^{2,0} \left[\frac{1}{a_2} \sqrt{\frac{x}{\bar{P}_r}} \middle| \begin{matrix} -; a_3 + 1 \\ a_5 + 1, a_4 + 1; - \end{matrix} \right], x \geq 0. \quad (24)$$

The result obtained in Proposition 2 and the expression given in (24) enable us to derive the statistical characterization of the BRT. It can be observed from Proposition 2 and (24) that the received power depends on the number of RIS elements N , the transmission power, and the propagation distance. Accordingly, we expect that the BRT will also depend directly on those parameters, as will be discussed next.

III. BATTERY RECHARGING TIME STATISTICAL MODELS

In this section, the statistical models developed in Section II are employed to derive analytical expressions for the statistical characterization of the instantaneous BRT, T_r , at the ER node.

In this paper, we adopt the BRT model presented in [49] and verified through experimental results in [50]. Specifically, the power harvested by the ER can be calculated as $P_h = P_r \eta$, where P_r is given in (2) and η is the RF to direct current conversion efficiency. The recharging current, I_b , of a battery can be calculated from P_h as $I_b = \frac{P_h}{V_b}$, where V_b is the constant operating voltage of the battery. Denoting C_b and D_d as the capacity of the battery and the discharge depth, respectively, the BRT can be expressed as

$$T_r = \frac{C_b D_d}{I_b} = \frac{C_b D_d V_b}{P_h} = \frac{C_b D_d V_b}{\eta P_r} = \frac{\alpha}{P_r}, \quad (25)$$

where $\alpha > 0$ denotes the conversion coefficient, which is a function of the battery and the RFEH circuit parameters and can be expressed as follows

$$\alpha = \frac{C_b D_d V_b}{\eta}. \quad (26)$$

It can be noticed that the BRT is inversely proportional to the conversion efficiency, η . Furthermore, when the battery capacity or the charging depth increases, the conversion coefficient, α , increases and the time required to charge the battery increases and vice versa. It is worth noting that the conversion efficiency, η , is different from the conversion coefficient, α . In this sense, η does not depend on the battery characteristic, i.e., capacity and discharge depth, but rather depends on the characteristics of the RF-to-DC conversion circuitry.

In this section, we exploit the PDF and CDF of the instantaneous received power, derived in (24) and (18), respectively, to obtain the statistical distribution of the BRT of a RIS-assisted WPT system.

A. Probability Density Function (PDF) of the BRT

The following proposition offers a closed-form expression for the PDF of the BRT in an RIS-aided WPT system.

Proposition 3: For RIS-assisted WPT systems, the PDF of the BRT at the ER node is given as

$$f_{T_r}(\tau) \approx \frac{a_1 a_2}{2\tau} G_{1,2}^{2,0} \left[\frac{1}{a_2} \sqrt{\frac{\alpha}{\bar{P}_r \tau}} \middle| \begin{array}{c} -; a_3 + 1 \\ a_5 + 1, a_4 + 1; - \end{array} \right], \tau > 0. \quad (27)$$

Proof: Using (25) and with the help of the Jacobian transformation method [66], the PDF of T_r is given as

$$f_{T_r}(\tau) = \frac{\alpha}{\tau^2} f_{P_r} \left(\frac{\alpha}{\tau} \right), \quad (28)$$

which, with the aid of (24), can be expressed in a closed-form expression as in (27). This completes the proof. ■

It is worth noting that (27) is simple and incorporates the Meijer G-function, which is a standard built-in function in most of the well-known mathematical software packages, such as MATLAB, MAPLE, and MATHEMATICA, and can, therefore, be efficiently evaluated.

B. Cumulative Distribution Function (CDF) of the BRT

The CDF of the BRT is defined as the probability that the instantaneous BRT falls below a predetermined threshold, τ_{th} , i.e., $F_{T_r}(\tau_{th}) = P(\tau \leq \tau_{th})$. Taking into account (25), it is straightforward to note that the relation between the CDFs of the received power and the BRT is

$$F_{T_r}(\tau_{th}) \approx 1 - F_{P_r} \left(\frac{\alpha}{\tau_{th}} \right). \quad (29)$$

Therefore, by substituting (18) into (29), we obtain the CDF of the BRT in a closed-form expression as

$$F_{T_r}(\tau_{th}) = 1 - a_1 a_2 G_{2,3}^{2,1} \left[\frac{1}{a_2} \sqrt{\frac{\alpha}{\bar{P}_r \tau_{th}}} \middle| \begin{array}{c} 1; a_3 + 1 \\ a_4 + 1, a_5 + 1; 0 \end{array} \right], \tau_{th} > 0. \quad (30)$$

C. BRT Mean Value, Variance, Skewness, Kurtosis, and AoF

The n -th order moment of the BRT, denoted by $\mu_{T_r}(n)$, is a very useful statistical tool, as it enables the characterization of the mean value of the BRT, in addition to other underlying useful properties such as its skewness and kurtosis. Moreover, it can be employed to quantify the AoF, as is elaborated next.

Having (27) in hand, we can derive the n -th moment of the BRT through the n -th order statistical expectation, as presented in the following proposition.

Proposition 4: The n -th moment of the BRT of an RIS-assisted WPT system can be expressed in a simple closed-form

expression as

$$\mu_{T_r}(n) \approx a_1 a_2^{(1-2n)} \left(\frac{\alpha}{\bar{P}_r} \right)^n \frac{\Gamma(a_4 + 1 - 2n) \Gamma(a_5 + 1 - 2n)}{\Gamma(a_3 + 1 - 2n)}. \quad (31)$$

Proof: The n -th moment of T_r can be evaluated by taking the statistical expectation

$$\mu_{T_r}(n) = \int_0^\infty \tau^n f_{T_r}(\tau) d\tau. \quad (32)$$

Then, by substituting (27) in (32), we obtain

$$\mu_{T_r}(n) = \frac{a_1 a_2}{2} \mathcal{J} \quad (33)$$

where

$$\mathcal{J} = \int_0^\infty \tau^{n-1} G_{1,2}^{2,0} \left[\frac{1}{a_2} \sqrt{\frac{\alpha}{\bar{P}_r \tau}} \middle| \begin{array}{c} -; a_3 + 1 \\ a_5 + 1, a_4 + 1; - \end{array} \right] d\tau. \quad (34)$$

By applying [65, Eq. (07.34.21.0009.01)] to solve the integral \mathcal{J} , (31) is obtained. This completes the proof. ■

The expression in (31) can be used to obtain the mean value of the BRT, \bar{T}_r , by setting $n = 1$, i.e., $\bar{T}_r = \mu_{T_r}(1)$. Also, the variance, $\sigma_{T_r}^2$, can be computed as

$$\sigma_{T_r}^2 = \mu_{T_r}(2) - \bar{T}_r^2. \quad (35)$$

The AoF parameter is viewed as a unified statistical measure of the severity of fading. Therefore, it is useful in quantifying the robustness of RIS-assisted WPT links against the channel fading. The AoF is defined in [67, Eq.(1.27)] as the ratio of the variance to the square mean of the instantaneous received power. Therefore, by employing (31), $AoF = \sigma_{T_r}^2 / \bar{T}_r^2$.

Remark: By examining (31), when n is set to 1, we note that the scaling law of the mean value of the BRT as a function of the RIS distances from the source and the ER nodes, denoted as d_1 and d_2 , and implicitly defined through \bar{P}_r in (22), dictates that \bar{T}_r increases with the square of the product of the distances d_1 and d_2 . This suggests that the minimum value of \bar{T}_r is achieved when the RIS is located either closer to the source or the ER node.

In addition to the mean and variance of the BRT, statistical properties such as the skewness, denoted by ϵ , and the kurtosis, denoted by Ψ , can be evaluated from (31) to provide deeper insights on the distribution of the BRT. More specifically, the skewness measures the asymmetry of the PDF of the BRT about its mean value, while the kurtosis is an indicator of its peakedness or flatness and the heaviness of its tail. The skewness is defined as [66]

$$\epsilon = \frac{\mu_{T_r}(3)}{\mu_{T_r}^{3/2}(2)}, \quad (36)$$

while the kurtosis is defined as

$$\Psi = \frac{\mu_{T_r}(4)}{\mu_{T_r}^2(2)} - 3. \quad (37)$$

Special Case: In the special case when the RIS consists of an asymptotically large number of RIS elements ($N \gg 1$), the following lemma returns a closed-form expression for the PDF

$$f_{\tau_r}(\tau) = \frac{2\alpha}{\tau^2 N (16 - \pi^2) \bar{P}_r} \left(\frac{\tau N^2 \pi^2 \bar{P}_r}{4\alpha} \right)^{\frac{1}{4}} \exp \left(-\frac{(4\alpha/\tau) + N^2 \pi^2 \bar{P}_r}{2N (16 - \pi^2) \bar{P}_r} \right) I_{-\frac{1}{2}} \left(\frac{2\pi}{(16 - \pi^2) \bar{P}_r} \sqrt{\bar{P}_r \alpha} \right), \tau > 0. \quad (38)$$

$$f_{P_r}(x) = \frac{2}{N (16 - \pi^2) \bar{P}_r} \left(\frac{N^2 \pi^2 \bar{P}_r}{4x} \right)^{\frac{1}{4}} \exp \left(-\frac{4x + N^2 \pi^2 \bar{P}_r}{2N (16 - \pi^2) \bar{P}_r} \right) I_{-\frac{1}{2}} \left(\frac{2\pi}{(16 - \pi^2) \bar{P}_r} \sqrt{\bar{P}_r x} \right), x \geq 0 \quad (43)$$

of the BRT for WPT systems.

Lemma 1: For a sufficiently large number of RIS elements $N \gg 1$, the PDF of the BRT for an RIS-assisted WPT system can be expressed in a closed-form expression as in (38), which is shown at the top of this page.

Proof: Recalling that $|h_i|$ and $|g_i|$ are independently distributed Rayleigh RVs, the mean and variance of B_i are, respectively, given as

$$\mathbb{E}[B_i] = \mathbb{E}[|h_i||g_i|] = \frac{\pi}{2} \quad (39)$$

and

$$\text{VAR}[B_i] = \left(\frac{16 - \pi^2}{4} \right). \quad (40)$$

As the number of RIS elements becomes sufficiently large, according to the CLT, B converges to a Gaussian distribution with mean

$$\mu_N = \mathbb{E}[B] = \frac{N\pi}{2} \quad (41)$$

and variance

$$\sigma_N^2 = N \left(\frac{16 - \pi^2}{4} \right), \quad (42)$$

where μ_N and σ_N^2 can be deduced by using (13) and (14). As a result, the instantaneous received power at the ER, P_s , defined in (2), has a non-central chi-square distribution with one degree of freedom [68], and its PDF is given in (43), shown at the top of this page, where $I_v(\cdot)$ is the modified Bessel function of order v defined in [62, Eq. (9.6.20)]. Finally, The expression in (38) can be obtained by inserting (43) into (28). This completes the proof. ■

Based on Lemma 1 and using (38), the mean value of the BRT when $N \gg 1$ converges to

$$\bar{T}_r = \mathbb{E}[\tau_r] = \frac{4\alpha}{(N^2 \pi^2 + N(16 - \pi^2)) \bar{P}_r}. \quad (44)$$

By a direct inspection of (44), we note that the mean value of the BRT in RIS-assisted WPT systems is shown to be inversely proportional to the square of the total number of RIS elements N , i.e., $\mathbb{E}[\tau_r] \propto \frac{1}{N^2 \bar{P}_r}$. This result is in agreement with the BRT definition given in (25).

IV. NUMERICAL AND SIMULATION RESULTS

In this section, numerical and Monte Carlo simulation results are presented to validate the accuracy of the proposed theoretical framework. This section also focuses on characterizing the properties of the BRT in RIS-assisted WPT systems. The term Monte Carlo simulations refers to the use of the

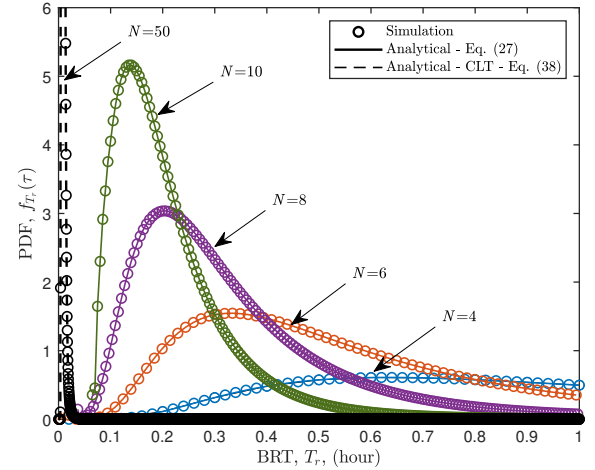


Figure 2: The PDF of the BRT of an RIS-assisted WPT system, for different values of N , where the transmit power, $P_s = 15$ dBm. The PDFs obtained through the CLT are also plotted for $N = 10$ and 50 .

actual fading channels with a number of realizations of 10^6 trials.

Unless otherwise stated, the RFEH efficiency factor is equal to $\eta = 0.5$, and it represents a worst case scenario, capturing the effects of low-cost hardware, and the total distance, d_{tot} , between the source node, S , and the ER node is set to 5 m. In order to ensure far-field conditions, we assume that the size of the RIS is relatively smaller than the transmission distance. It is assumed that the RIS is located mid-way between S and the ER, i.e., $d_1 = d_2 = d_{tot}/2$, and the path loss exponent, $\delta = 2.7$ [11]. All simulation parameters, including the ER battery parameters, are summarized in Table 1.

Table I: Simulation Parameters.

Name	Symbol	Value
RFEH efficiency of the ER circuit	η	0.5
Normalized $S \rightarrow$ RIS distance	d_1/d_{tot}	0.5
Normalized RIS \rightarrow ER distance	d_2/d_{tot}	0.5
Path loss exponent	δ	2.7
Battery capacity	C_b	10 mAh
Discharge depth	D_d	0.4
Battery charging voltage	V_b	1.2 V

In Fig. 2, the PDF of the BRT for RIS-assisted WPT systems is illustrated for different values of the RIS elements N , by using the analytical expression given in (27), where $N = 4, 6, 8, 10, 50$. Additionally, the PDF of the BRT obtained

through the CLT, as given in (38), is also shown for $N = 10$ and 50. It is observed that the simulation results are in good agreement with the analytical PDF curves, which substantiates the accuracy of the proposed mathematical model and its effectiveness in capturing the statistical properties of the BRT. Additionally, we note that the BRT of the ER node decreases as N increases. In more details, the highest probable value of the BRT drops from 0.64 to 0.2 hr (38.4 to 12 mins) when the number of RIS elements increases from 4 to 8. Finally, it is evident that, as the number of RIS elements increases, the PDF converges to an impulse function, indicating that increasing N causes a significant reduction of the BRT of WPT systems, due to the enhanced passive beamforming gain of RIS-assisted systems, which make them particularly attractive for large-scale RFEH applications. It is worth mentioning that the effect of increasing the number of RF sources on the BRT was studied in [50]. Although the results in [50] demonstrated that the BRT decreases notably by increasing the number of RF sources, this comes at the cost of extra transmission power that is needed for each additional RF source.

In Fig. 3, we investigate the effect of varying the value of the transmit power, P_s , on the BRT performance of RIS-assisted WPT systems. We plot the PDF of the BRT when $N = 4, 6,$ and 8 , by using the analytical expression in (27). Figs. (3a), (3b), and (3c) present, respectively, low, moderate, and high transmit power regimes, i.e., $P_s = 7, 15,$ and 40 dBm. By closely inspecting these figures, it is clearly observed that, when the transmit power is high, the variance of the distribution of the BRT decreases while its kurtosis increases (i.e., sharper PDF peak), indicating the improvement in the BRT predictability. Interestingly, it can be noted that, even in the low transmit power scenario, depicted in Fig. 3a, the mean value of the BRT exhibits high predictability when $N = 8$ compared to the cases when $N = 4$ and 6 . This indicates that the deployment of an RIS is promising in enhancing the reliability of WPT, and may be attained by adding low-cost passive RIS elements (featuring no transmit power consumption) instead of increasing the source transmission power. Further details about this aspect are given next.

To gain more insights about the effect of varying the transmit power on the statistical distribution of the BRT in RIS-assisted WPT systems, we illustrate in Fig. 4 the CDF as a function of the BRT threshold, τ_{th} , of an RIS-assisted system by using (29). The analysis is carried out for different values of N and assuming two transmit power scenarios, namely low- ($P_s = 7$ dBm) and high- ($P_s = 20$ dBm) transmit power. The excellent fit between the simulation and the analytical results verify the accuracy of the developed theoretical framework. As expected, for a fixed N , as τ_{th} increases, the CDF value increases. For example, the CDF value approximately doubles for $N = 4$ and $P_s = 7$ dBm, as τ_{th} changes from 5 to 10 hrs. Additionally, for a given τ_{th} value, as N increases, the CDF value improves. This indicates that the efficiency of the RFEH process is improved in an RIS-assisted WPT system by increasing the number of RIS elements N . For instance, at $P_s = 7$ dBm, τ_{th} can be reduced by about 4 hrs by employing an RIS with 8 elements instead of 6 in order to achieve a targeted probability of charging equal to 0.9. Fig. 4 also

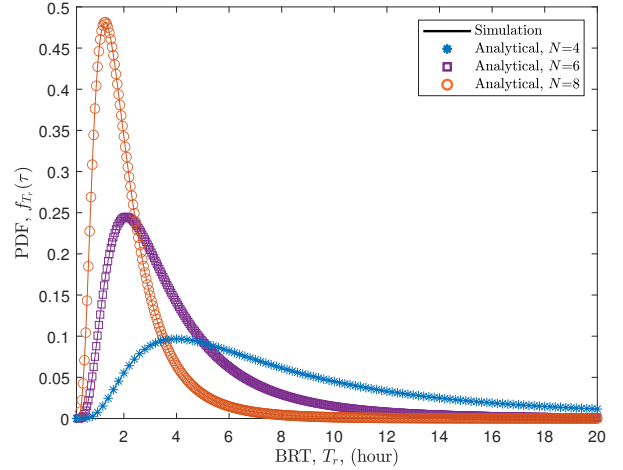
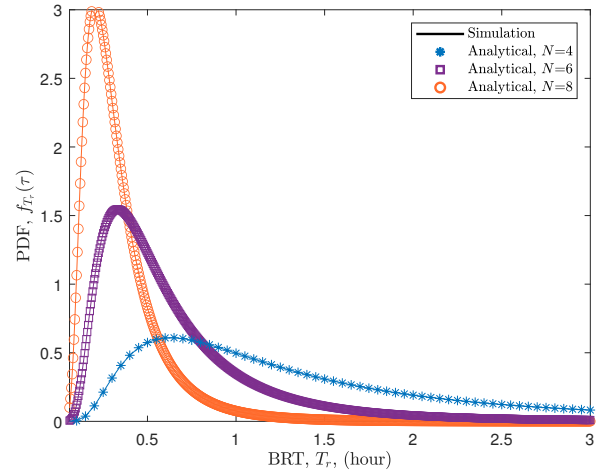
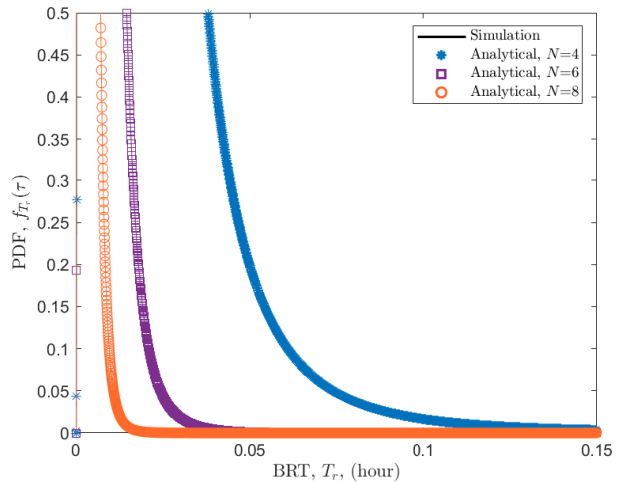
(a) $P_s = 7$ dBm(b) $P_s = 15$ dBm(c) $P_s = 40$ dBm

Figure 3: The PDF of the BRT in RIS-assisted WPT systems, in (a) low transmit power, $P_s = 7$ dBm, (b) moderate transmit power, $P_s = 15$ dBm, and (c) high transmit power, $P_s = 40$ dBm, regimes, and for different values of N .

demonstrates that the steepness of the CDF curve increases as the value of the transmit power shifts from low to high. This

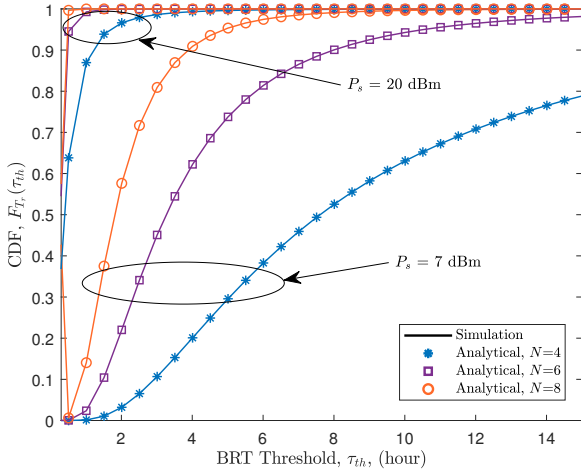


Figure 4: The CDF as a function of BRT threshold for RIS-assisted for low- and high- transmit power scenarios and for different values of N .

indicates that adding more RIS elements is more rewarding in the low transmit power than the high transmit power regime, where the reduction in the BRT value is more significant.

Fig. 5 depicts the mean value of the BRT, \bar{T}_r , as a function of the total transmit power, P_s , for different values of N . We also examine the convergence of the mean value, obtained analytically in (31), towards that obtained through the CLT, given in (44). It can be deduced from Fig. 5 that \bar{T}_r converges to the mean value computed via the CLT even for relatively small values of N , e.g., when $N > 8$. This suggests that the mean value of the BRT in RIS-assisted WPT systems can be mathematically evaluated using the simpler expressions in (44) instead of (31), which is computationally more demanding, since it involves the evaluation of the parameters a_1 through a_5 . We further notice that, as N and P_s increase, the mean value of the BRT linearly decreases. This finding is in agreement with the theoretical result obtained in (44). In more detail, for a given value of P_s , doubling the number of deployed RIS elements N yields a reduction of the mean value of the BRT by about 4 times. In summary, the choice of N depends on whether the application scenario operates in the low or high transmit power scenarios.

Remark: We emphasize that the analytical expressions derived in (31) and (44) constitute effective tools in determining the minimum number of RIS elements that should be deployed in order to achieve a feasible BRT for a targeted energy efficiency in WPT systems, while avoiding the need of unnecessary phase adjustments to account for extra deployed RIS elements.

To examine the BRT performance under NLoS propagation in comparison to scenarios in which LoS propagation is established, Fig. 6 compares the mean value of the BRT, \bar{T}_r , as a function of the transmit power for the two cases of Rayleigh fading (i.e., NLoS only) and Rician fading [67] (i.e., LoS + NLoS). For the latter case, we assume that each of $|h_i|$ and $|g_i|$ in (3) follows a Rician distribution with shaping parameters K_1 and K_2 , respectively. We further assume that $K_1 = K_2 = K = \frac{v^2}{2\sigma^2}$, where v^2 and $2\sigma^2$ represent the power

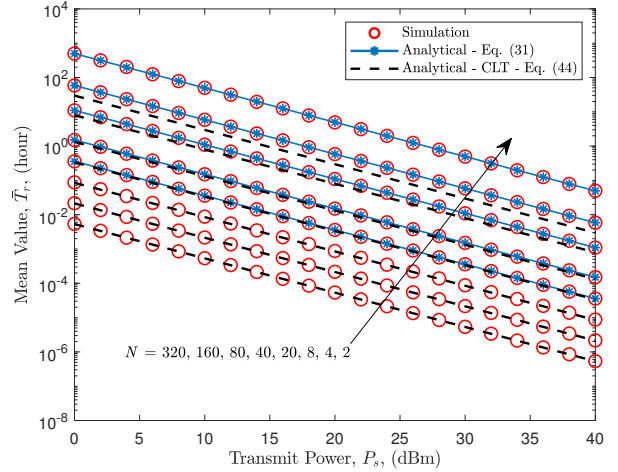


Figure 5: Mean value of the BRT as a function of the transmit power in RIS-assisted WPT systems, for different values of N .

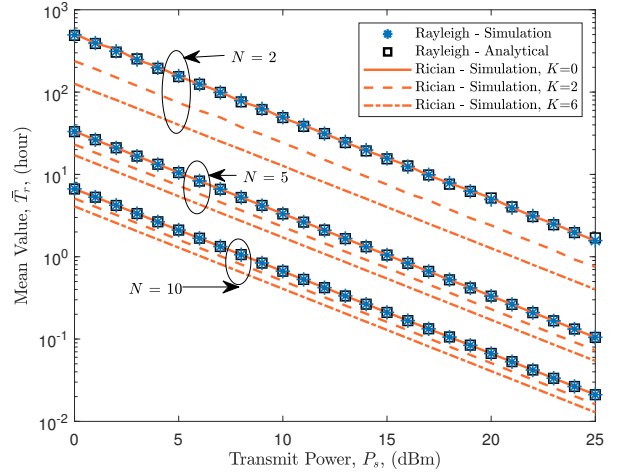


Figure 6: Mean value of the BRT as a function of the transmit power in RIS-assisted WPT systems over Rayleigh fading in comparison with Rician Fading.

of the LoS component and NLoS components, respectively. It can be observed from Fig. 6 that, as the value of K increases (i.e., the LoS component is stronger), the mean time required to charge the battery reduces. Moreover, Fig. 6 demonstrates that increasing the number of elements, N , compensates for worse fading conditions. This is more noticeable for higher values of N , e.g., $N = 10$ compared to $N = 2$.

To quantify the impact of the RIS location on the BRT performance, in Fig. 7, we inspect the behavior of the mean value of the BRT, \bar{T}_r , as a function of the normalized $S \rightarrow$ RIS distance, d_1/d_{tot} , for different values of N and for $P_s=20$ dBm. We set the normalized RIS \rightarrow ER distance to $d_2/d_{tot} = 1 - d_1/d_{tot}$. It is noted that, for a given RIS location, the energy efficiency of a WPT system can be enhanced by equipping the RIS with more elements. This key BRT performance insight is beneficial when there is no flexibility in choosing the location of the RIS due to the layout or geometry of the environment. Additionally, it is observed that

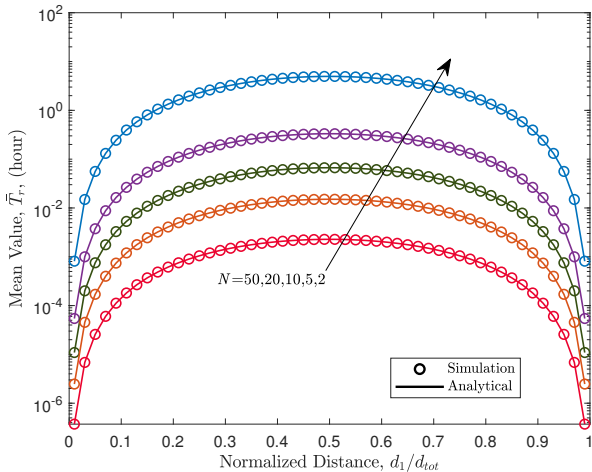


Figure 7: Mean value of the BRT as a function of the normalized $S \rightarrow$ RIS distance, d_1/d_{tot} , for RIS-assisted WPT systems, for different values of N and $P_s = 20$ dBm.

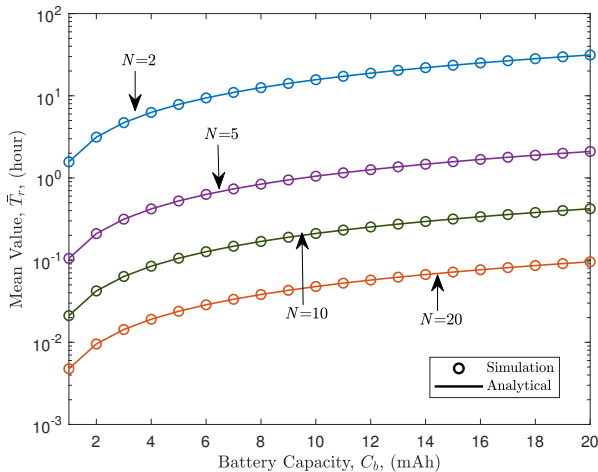


Figure 8: Mean value of the BRT as a function of the battery capacity of the ER node in RIS-assisted WPT systems, for different values of N and when $P_s = 20$ dBm.

the minimum mean value of the BRT is attained when the RIS is located either closer to S or closer to the ER node. This verifies the findings in Sec. III-C based on (31).

To address the effect of varying the battery parameters, in Fig. 8 we plot the mean value of the BRT, \bar{T}_r , with respect to the battery capacity, C_b , of the ER node when the transmit power is fixed to 20 dBm. As expected, for a given N , it is observed that, as C_b increases, the mean value of the BRT increases. In addition, the figure reveals that, independently of C_b , as N doubles, \bar{T}_r decreases by about 5 times. For example, for $C_b = 10$ mAh, as N is varied from 5 to 10 to 20, the mean value of the BRT is reduced from 1 hr to 12.65 mins to 2.86 mins. This finding can be of considerable advantage for applications where the battery capacity is determined by constraints on the shape and size of the RFEH nodes, such as wearables or implantables.

Finally, in Fig. 9, we examine the AoF for RIS-assisted

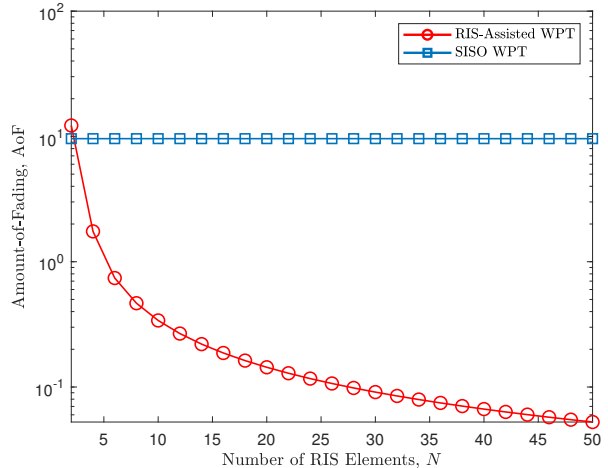


Figure 9: AoF as a function of N when $P_s = 20$ dBm.

WPT systems as a function of the number of RIS elements N . We also plot the AoF for a single-input single-output (SISO) WPT system as a benchmark. Fig. 9 shows that the proposed analytical framework is useful in quantifying the robustness of RIS-assisted WPT to fading channels. Particularly, Fig. 9 reveals that increasing N reduces the AoF of the E2E channel, thereby improving the efficiency of WPT in fading channels.

V. CONCLUSION

In this paper, we developed a theoretical framework to investigate the energy sustainability of RIS-assisted WPT systems, from the BRT perspective of an RFEH node. In particular, over Rayleigh fading channels, we provided the statistical characterization of the instantaneous received power of the system, including its PDF and CDF. Based on that, we derived novel low-complexity tight closed-form approximations for the PDF, CDF, and moments of the BRT as a function of the received power, battery parameters, and number of RIS elements. Additionally, using the CLT, we derived closed-form expressions for the PDF and mean value of the BRT considering that the RIS is equipped with a large number of elements. Besides being accurate and mathematically tractable, our results reveal that the proposed statistical tools constitute an efficient means to evaluate the performance of RIS-assisted WPT systems and extract useful design insights. For example, our results show that doubling the number of RIS elements improves the predictability of the BRT of the RFEH nodes and offers a 4-fold reduction in its mean value. Moreover, it is reported that the characteristics of the BRT are impacted not only by the system parameters, such as the distance between the nodes, but also by the battery parameters of the RFEH node, such as the battery capacity. Finally, our results illustrated that significant performance gains in the BRT can be obtained by deploying the RIS closer to the source or closer to the RFEH node [69].

REFERENCES

- [1] M. Di Renzo *et al.*, "Smart radio environments empowered by reconfigurable AI meta-surfaces: an idea whose time has come," *EURASIP J. Wireless Commun. Netw.*, vol. 2019, no. 1, pp. 1–20, May 2019.

- [2] E. Basar *et al.*, "Wireless communications through reconfigurable intelligent surfaces," *IEEE Access*, vol. 7, pp. 116753–116773, Aug. 2019.
- [3] C. Liaskos *et al.*, "A new wireless communication paradigm through software-controlled metasurfaces," *IEEE Commun. Mag.*, vol. 56, no. 9, pp. 162–169, Sept. 2018.
- [4] Q. Wu and R. Zhang, "Towards smart and reconfigurable environment: Intelligent reflecting surface aided wireless network," *IEEE Commun. Mag.*, vol. 58, no. 1, pp. 106–112, Jan. 2020.
- [5] L. Bariah *et al.*, "A prospective look: Key enabling technologies, applications and open research topics in 6G networks," *IEEE Access*, vol. 8, pp. 174792–174820, Aug. 2020.
- [6] F. Tariq *et al.*, "A speculative study on 6G," *IEEE Wireless Commun.*, vol. 27, no. 4, pp. 118–125, Aug. 2020.
- [7] L. R. Varshney, "Transporting information and energy simultaneously," in *Proc. IEEE Int. Symp. Inf. Theory*, Toronto, Canada, July 2008, pp. 1612–1616.
- [8] P. Grover and A. Sahai, "Shannon meets tesla: Wireless information and power transfer," in *Proc. IEEE Int. Symp. Int. Theory (ISIT'10)*, June 2010, pp. 2363–2367.
- [9] S. Bi, C. K. Ho, and R. Zhang, "Wireless powered communication: opportunities and challenges," *IEEE Commun. Mag.*, vol. 53, no. 4, pp. 117–125, Apr. 2015.
- [10] L. Mohjazi *et al.*, "RF-powered cognitive radio networks: technical challenges and limitations," *IEEE Commun. Mag.*, vol. 53, no. 4, pp. 94–100, Apr. 2015.
- [11] L. Mohjazi *et al.*, "Performance analysis of SWIPT relaying systems in the presence of impulsive noise," *IEEE Access*, vol. 6, pp. 71662–71677, Nov. 2018.
- [12] L. Mohjazi, S. Muhaidat, M. Dianati, and M. Al-Qutayri, "Performance analysis of SWIPT relay networks with noncoherent modulation," *IEEE Trans. Green Commun. Netw.*, vol. 2, no. 4, pp. 1072–1086, Dec. 2018.
- [13] A. Nasir, X. Zhou, S. Durrani, and R. Kennedy, "Relaying protocols for wireless energy harvesting and information processing," *IEEE Trans. Wireless Commun.*, vol. 12, no. 7, pp. 3622–3636, July 2013.
- [14] B. Yang *et al.*, "Digital beamforming-based massive MIMO transceiver for 5G millimeter-wave communications," *IEEE Trans. Microw. Theory Techn.*, vol. 66, no. 7, pp. 3403–3418, July 2018.
- [15] E. G. Larsson and H. V. Poor, "Joint beamforming and broadcasting in massive MIMO," *IEEE Trans. Wireless Commun.*, vol. 15, no. 4, pp. 3058–3070, Apr. 2016.
- [16] W. Hao *et al.*, "Beamforming design in SWIPT-based joint multicast-multicast mmWave massive MIMO with lens-antenna array," *IEEE Wireless Commun. Lett.*, vol. 8, no. 4, pp. 1124–1128, Aug. 2019.
- [17] L. Mohjazi *et al.*, "An outlook on the interplay of AI and software-defined metasurfaces," *IEEE Veh. Technol. Mag.*, vol. 15, no. 4, pp. 62–73, Dec. 2020.
- [18] H. Yang *et al.*, "A programmable metasurface with dynamic polarization, scattering and focusing control," *Scientific Reports*, vol. 6, p. 35692, Oct. 2016.
- [19] C. Huang *et al.*, "Holographic MIMO surfaces for 6G wireless networks: Opportunities, challenges, and trends," *IEEE Wireless Commun.*, vol. 27, no. 5, pp. 118–125, Oct. 2020.
- [20] M. Di Renzo *et al.*, "Smart radio environments empowered by reconfigurable intelligent surfaces: How it works, state of research, and road ahead," *IEEE J. Sel. Areas Commun.*, vol. 38, no. 11, pp. 2450–2525, Nov. 2020.
- [21] M. Dunna, C. Zhang, D. Stevenpiper, and D. Bharadia, "ScatterMIMO: enabling virtual MIMO with smart surfaces," in *Proc. Int. Conf. Mobile Computing and Networking (MobiCom'20)*, Apr. 2020, pp. 1–14.
- [22] V. Arun and H. Balakrishnan, "RFocus: Beamforming using thousands of passive antennas," in *USENIX NS*, Feb. 2020, pp. 1047–1061.
- [23] K. Ntontin *et al.*, "Reconfigurable intelligent surfaces vs. relaying: Differences, similarities, and performance comparison," *IEEE Open J. Commun. Soc.*, vol. 1, pp. 798–807, June 2020.
- [24] C. Huang *et al.*, "Reconfigurable intelligent surfaces for energy efficiency in wireless communication," *IEEE Trans. Wireless Commun.*, vol. 18, no. 8, pp. 4157–4170, Aug. 2019.
- [25] Y. Yang, S. Zhang, and R. Zhang, "IRS-enhanced OFDM: Power allocation and passive array optimization," in *Proc. IEEE Global Commun. Conf. (GLOBECOM)*, Waikoloa, HI, USA, 2019, pp. 1–6.
- [26] Q. Nadeem *et al.*, "Intelligent reflecting surface assisted multi-user MISO communication: Channel estimation and beamforming design," *IEEE Open J. Commun. Soc.*, vol. 1, pp. 661–680, May 2020.
- [27] A. Zappone *et al.*, "Overhead-aware design of reconfigurable intelligent surfaces in smart radio environments," *IEEE Trans. Wireless Commun.*, vol. 20, no. 1, pp. 126–141, Sept. 2020.
- [28] Y. Yang, B. Zheng, S. Zhang, and R. Zhang, "Intelligent reflecting surface meets OFDM: Protocol design and rate maximization," *IEEE Trans. Commun.*, vol. 68, no. 7, pp. 4522–4535, Mar. 2020.
- [29] E. Basar, "Reconfigurable intelligent surface-based index modulation: A new beyond MIMO paradigm for 6G," *IEEE Trans. Commun.*, vol. 68, no. 5, pp. 3187–3196, Feb. 2020.
- [30] L. Zhang *et al.*, "Space-time-coding digital metasurfaces," *Nature Commun.*, vol. 9, no. 1, pp. 1–11, Oct. 2018.
- [31] M. Jung *et al.*, "Reliability analysis of large intelligent surfaces (LISs): Rate distribution and outage probability," *IEEE Wireless Commun. Lett.*, vol. 8, no. 6, pp. 1662–1666, Dec. 2019.
- [32] M. Di Renzo and J. Song, "Reflection probability in wireless networks with metasurface-coated environmental objects: an approach based on random spatial processes," *EURASIP J. Wireless Commun. Netw.*, vol. 2019, no. 1, p. 99, Apr. 2019.
- [33] M. Jung, W. Saad, and G. Kong, "Spectral efficiency in large intelligent surfaces: Asymptotic analysis under pilot contamination," in *Proc. IEEE Global Commun. Conf. (GLOBECOM)*, Waikoloa, HI, USA, 2019, pp. 1–6.
- [34] S. Zhou *et al.*, "Spectral and energy efficiency of IRS-assisted MISO communication with hardware impairments," *IEEE Wireless Commun. Lett.*, vol. 9, no. 9, pp. 1366–1369, Sept. 2020.
- [35] S. Zhang and R. Zhang, "Capacity characterization for intelligent reflecting surface aided MIMO communication," *IEEE J. Sel. Areas Commun.*, vol. 38, no. 8, pp. 1823–1838, Aug. 2020.
- [36] R. Karasik, O. Simeone, M. Di Renzo, and S. Shamai, "Beyond max-SNR: Joint encoding for reconfigurable intelligent surfaces," in *IEEE Int. Symp. Inf. Theory (ISIT'20)*, June 2020, pp. 2965–2970.
- [37] N. S. Perović, M. Di Renzo, and M. F. Flanagan, "Channel capacity optimization using reconfigurable intelligent surfaces in indoor mmWave environments," in *IEEE Int. Conf. Commun. (ICC'20)*, Dublin, Ireland, 2020, pp. 1–7.
- [38] W. Zhao *et al.*, "Performance analysis of large intelligent surface aided backscatter communication systems," *IEEE Wireless Commun. Lett.*, vol. 9, no. 7, pp. 962–966, July 2020.
- [39] V. C. Thirumavalavan and T. S. Jayaraman, "BER analysis of reconfigurable intelligent surface assisted downlink power domain NOMA system," in *Proc. Int. Conf. Commun. Syst. Netw. (COMSNETS)*, Bengaluru, India, 2020, pp. 519–522.
- [40] Z. Chu, W. Hao, P. Xiao, and J. Shi, "Intelligent reflecting surface aided multi-antenna secure transmission," *IEEE Wireless Commun. Lett.*, vol. 9, no. 1, pp. 108–112, Jan. 2020.
- [41] Y. Zhang, C. Zhong, Z. Zhang, and W. Lu, "Sum rate optimization for two way communications with intelligent reflecting surface," *IEEE Commun. Lett.*, vol. 24, no. 5, pp. 1090–1094, May 2020.
- [42] Q. Wu and R. Zhang, "Intelligent reflecting surface enhanced wireless network via joint active and passive beamforming," *IEEE Trans. Wireless Commun.*, vol. 18, no. 11, pp. 5394–5409, Nov. 2019.
- [43] H. Han *et al.*, "Intelligent reconfigurable surface aided power control for physical-layer broadcasting," *arXiv:1912.03468*, 2019.
- [44] G. Zhou *et al.*, "Robust beamforming design for intelligent reflecting surface aided MISO communication systems," *IEEE Wireless Commun. Lett.*, vol. 9, no. 10, pp. 1658–1662, Oct. 2020.
- [45] H. Lang and C. D. Sarris, "Optimization of wireless power transfer systems enhanced by passive elements and metasurfaces," *IEEE Trans. Antennas Propag.*, vol. 65, no. 10, pp. 5462–5474, Oct. 2017.
- [46] Q. Wu and R. Zhang, "Weighted sum power maximization for intelligent reflecting surface aided SWIPT," *IEEE Wireless Commun. Lett.*, vol. 9, no. 5, pp. 586–590, May 2020.
- [47] C. Pan *et al.*, "Intelligent reflecting surface aided MIMO broadcasting for simultaneous wireless information and power transfer," *IEEE J. Sel. Areas Commun.*, vol. 38, no. 8, pp. 1719–1734, Aug. 2020.
- [48] Q. Wu and R. Zhang, "Joint active and passive beamforming optimization for intelligent reflecting surface assisted SWIPT under QoS constraints," *IEEE J. Sel. Areas Commun.*, vol. 38, no. 8, pp. 1735–1748, July 2020.
- [49] D. Altinel and G. K. Kurt, "Statistical models for battery recharging time in rf energy harvesting systems," in *Proc. IEEE Wireless Commun. Netw. Conf. (WCNC)*, Istanbul, Turkey, Apr. 2014, pp. 636–641.
- [50] D. Altinel and G. Karabulut Kurt, "Energy harvesting from multiple RF sources in wireless fading channels," *IEEE Trans. Veh. Technol.*, vol. 65, no. 11, pp. 8854–8864, Nov. 2016.
- [51] E. Salahat and N. Yang, "Statistical models for battery recharge time from RF energy scavengers in generalized wireless fading channels," in *Proc. IEEE Globecom Workshops (GC Wkshps)*, Singapore, 2017, pp. 1–6.

- [52] A. A. Boulogeorgos and A. Alexiou, "Performance analysis of reconfigurable intelligent surface-assisted wireless systems and comparison with relaying," *IEEE Access*, vol. 8, pp. 94 463–94 483, May 2020.
- [53] S. Atapattu *et al.*, "Reconfigurable intelligent surface assisted two-way communications: Performance analysis and optimization," *IEEE Trans. Commun.*, vol. 68, no. 10, pp. 6552–6567, Oct. 2020.
- [54] N. S. Perović, L.-N. Tran, M. Di Renzo, and M. F. Flanagan, "Achievable rate optimization for MIMO systems with reconfigurable intelligent surfaces," *IEEE Trans. Wireless Commun.*, vol. 20, no. 6, pp. 3865–3882, June 2021.
- [55] T. Van Chien, H. Q. Ngo, S. Chatzinotas, M. Di Renzo, and B. Ottersten, "Reconfigurable intelligent surface-assisted cell-free massive MIMO systems over spatially-correlated channels," *arXiv preprint arXiv:2104.08648*, 2021.
- [56] X. Qian *et al.*, "Beamforming through reconfigurable intelligent surfaces in single-user MIMO systems: SNR distribution and scaling laws in the presence of channel fading and phase noise," *IEEE Wireless Commun. Lett.*, vol. 10, no. 1, pp. 77–81, Jan. 2021.
- [57] T. Hou *et al.*, "Reconfigurable intelligent surface aided NOMA networks," *IEEE J. Sel. Areas Commun.*, vol. 38, no. 11, pp. 2575–2588, Nov. 2020.
- [58] W. Tang *et al.*, "Wireless communications with reconfigurable intelligent surface: Path loss modeling and experimental measurement," *IEEE Trans. Wireless Commun.*, vol. 20, no. 1, pp. 421–439, Jan. 2021.
- [59] M. Di Renzo *et al.*, "Analytical modeling of the path-loss for reconfigurable intelligent surfaces—anomalous mirror or scatterer?" in *IEEE Int. Workshop Signal Process. Advances Wireless Commun. (SPAWC'20)*, Atlanta, GA, USA, Aug. 2020, pp. 1–5.
- [60] V. S. Asadchy *et al.*, "Perfect control of reflection and refraction using spatially dispersive metasurfaces," *Physical Review B*, vol. 94, no. 7, p. 075142, 2016.
- [61] A. P. Prudnikov, Y. A. Brychkov, and O. I. Marichev, *Integrals and Series*. Gordon and Breach Science Publishers, 1986, vol. 3.
- [62] M. Abramowitz, *Handbook of Mathematical Functions, With Formulas, Graphs, and Mathematical Tables*. USA: Dover Publications, Inc., 1974.
- [63] F. El Bouanani and D. B. da Costa, "Accurate closed-form approximations for the sum of correlated Weibull random variables," *IEEE Wireless Commun. Lett.*, vol. 7, no. 4, pp. 498–501, Aug. 2018.
- [64] L. Bariah *et al.*, "Large intelligent surface-assisted nonorthogonal multiple access for 6G networks: Performance analysis," *IEEE Internet Things J.*, vol. 8, no. 7, pp. 5129–5140, Apr. 2021.
- [65] [Online]. Available: <http://functions.wolfram.com/>
- [66] A. Papoulis, *Probability, Random Variables, and Stochastic Processes*. New York: McGraw-Hill, 3rd edition, 1991.
- [67] M. K. Simon and M.-S. Alouini, *Digital Communications over Fading Channels. A Unified Approach to Performance Analysis*. New York, NY: John Wiley and Sons, Inc., 2000.
- [68] J. G. Proakis, *Digital Communications*. New York: McGraw-Hill, 4th edition, 2000.
- [69] A. A. Al-Habob, O. A. Dobre, S. Muhaidat, and H. Vincent Poor, "Energy-efficient data dissemination using a UAV: An ant colony approach," *IEEE Wireless Commun. Lett.*, vol. 10, no. 1, pp. 16–20, Jan. 2021.